



Cite this: *CrystEngComm*, 2021, 23, 6045

Design of hierarchical SnSe₂ for efficient detection of trace NO₂ at room temperature†

Tingting Wang,^a You Wang,^{*ab} Shengliang Zheng,^b Quan Sun,^b Ruozen Wu^b and Juanyuan Hao ^{*b}

Layered tin diselenide (SnSe₂) has aroused widespread scientific interest by virtue of its exceptional chemical, physical, and electrical characteristics. The distinctive features of SnSe₂ enable it to be an ideal candidate for efficient detection of NO₂ at room temperature. Herein, hierarchical SnSe₂ assembled from thin nanosheets was designed and prepared through a facile solvothermal method. An ultralow detection limit (10 ppb) and considerable NO₂ sensing performance were obtained at room temperature. A sensor based on hierarchical SnSe₂ demonstrated a high response value of 1200% (triple that of SnSe₂ nanosheets) and short response/recovery time of 50/55 s toward 10 ppm NO₂. These remarkable sensing properties are uncommon in two-dimensional (2D) materials at room temperature. Additionally, the sensor exhibited superb selectivity, reliable reproducibility, and excellent long-term stability within 5 months. These enhanced sensing properties could be ascribed to the unique hierarchical structures, which possess large accessible space that enhances the adsorption and diffusion of gas molecules. This study offers a new strategy to improve the sensing performance of SnSe₂ through rational morphology and structure design.

Received 18th June 2021,
Accepted 20th July 2021

DOI: 10.1039/d1ce00804h

rsc.li/crystengcomm

1 Introduction

Nitrogen dioxide (NO₂), a typical toxic gas mainly produced from emissions from the burning of fossil fuel, plays a major role in the formation of ozone and acid rain.^{1–3} Continuous exposure to even parts per million (ppm) levels of NO₂ may lead to respiratory diseases such as emphysema and chronic bronchitis. The ambient air standard for NO₂ adopted by the U.S. Environmental Protection Agency (EPA) is set to 53 ppb. Besides, NO₂ can possibly be considered as a biomarker for identifying some diseases such as irritable bowel and pulmonary diseases.^{4,5} Therefore, high-sensitivity detection of trace amounts of NO₂ is essential for environmental governance and the protection of personal health. Additionally, with the advent of the Internet of Things (IoT), some specific requirements including low cost, ultralow power consumption, and simple operation conditions should also be satisfied to embed sensors into portable devices.^{6–8} Unfortunately, traditional gas sensors based on metal oxide semiconductors usually need high operating temperature (200–600 °C), which revokes their advantages in intended

possible applications of the IoT.^{9–11} Hence, there has been an increasing tendency for developing novel materials to fabricate room-temperature NO₂ gas sensors.

As an alternative, two-dimensional layered metal dichalcogenides (2D-LMDs) have attracted considerable attention for room-temperature NO₂ detection due to the merits of their unique crystal structure and notable electrical characteristics.^{12–18} In particular, SnSe₂ has been recently exploited as an effective gas sensor to overcome some specific challenges associated with LMDs (MoS₂, WSe₂, SnS₂, etc.), such as poor selectivity and sluggish sensing response.^{19–24} Concretely speaking, the typical Se–Sn–Se layered structure would provide the opportunity to achieve a large accessible space for the adsorption of target gas molecules.^{25,26} Besides, the remarkable electrical properties of SnSe₂, including a narrow bandgap of 1–2 eV and high intrinsic conductivity, could facilitate charge transfer during gas sensing.^{27,28} In particular, Sn and Se are earth-abundant and environmentally-friendly elements, which endows SnSe₂ with distinct superiority for the application fields of the IoT.^{29,30} These extraordinary features of SnSe₂ make it an ideal candidate for fabricating advanced gas sensors. However, research on SnSe₂ for gas sensing is in its infancy, and the sensing performance of SnSe₂-based gas sensors still has plenty of room to improve, especially for highly sensitive detection of trace NO₂ at room temperature.

The morphology and structure of semiconductors play an indispensable role in adjusting their sensing characteristics,

^a School of Chemistry and Chemical Engineering, Harbin Institute of Technology, Harbin 150001, China. E-mail: y-wang@hit.edu.cn

^b School of Materials Science and Engineering, Harbin Institute of Technology, Harbin 150001, China. E-mail: jyhao@hit.edu.cn

† Electronic supplementary information (ESI) available. See DOI: 10.1039/d1ce00804h

because sensing processes depend on the adsorption and reaction of target gas molecules on the surface of materials to account for changes in resistance.^{31,32} However, 2D materials readily stack together due to the electrostatic force between each pair of layers. Such densely restacked structures would obscure active sites and reduce the diffusion of detected gases, thereby weakening the intrinsic sensing performance. To solve this issue, an effective strategy is to construct hierarchical structures with a high specific surface area and well-defined interior voids, which would stabilize high active site dispersion and facilitate aid in gas adsorption and transport, thus greatly increasing the sensing response as well as shortening the response/recovery time of gas sensors.^{33–37} For instance, Liu *et al.* have prepared SnS₂ nanoflowers assembled from nanosheets for ultrasensitive ppb-level NO₂ detection.³⁸ Zhang *et al.* have synthesized hierarchical flower-like MoS₂ nanospheres which showed superb gas response capability and considerable response/recovery properties toward NO₂.³⁹ Li *et al.* have reported that hierarchical hollow MoS₂ microspheres built from nanosheets demonstrated enhanced NO₂ sensing response and better selectivity than smooth MoS₂ spheres.⁴⁰ Similarly, hierarchical SnSe₂ has been used as an ultrasensitive SERS substrate and a high-performance flexible piezoresistive pressure sensor.^{41,42} On this account, the rational design of SnSe₂ with an innovative structure might be an efficient approach to achieve enhanced gas sensing performance.

Herein, nanosheet-assembled SnSe₂ hierarchical structures were prepared through a low-cost and facile one-step solvothermal process. A comparative investigation in terms of gas sensing properties between as-synthesized flower-like SnSe₂ and SnSe₂ nanosheets was also performed. As expected, the fabricated hierarchical SnSe₂ sensor presented an ultrahigh response (resistance ratio = 1200%) and a short response/recovery time (50/55 s) toward 10 ppm NO₂ at room temperature, which are far better than those of SnSe₂ sheets. Besides, the sensor showed a trace detection limit of 10 ppb, reliable reproducibility, remarkable complete recovery, and outstanding selectivity. Our studies demonstrate that the hierarchical SnSe₂ could serve as a new suitable candidate for high-performance room-temperature gas sensing.

2 Experimental

2.1 Synthesis of SnSe₂ hierarchical nanostructures

SnSe₂ hierarchical nanostructures were synthesized *via* a one-step solvothermal strategy following a previously reported method.⁴³ Firstly, 0.2 mmol tin(IV) chloride pentahydrate (SnCl₄·5H₂O, 98%), 0.2 mmol selenium dioxide (SeO₂, 99.9%), and 200 μL 1-dodecanethiol (1-DDT, 98%) were added into 17 mL oleylamine (OAM, 80–90%). After continuous stirring for 5 min, the mixture was heated at 70 °C for 30 min to obtain a clear yellow coloured solution. Then, the above mixture was transferred to a Teflon-lined autoclave (25 mL) and subjected to a solvothermal process at 180 °C for 60 h. After naturally

cooling to room temperature, the obtained precipitate was washed three times with cyclohexane and ethanol by centrifugation (8000 rpm, 5 min), and then dried at 60 °C for several hours to achieve the final product.

Moreover, to probe the reaction mechanism of the SnSe₂ hierarchical nanostructures, time-dependent reactions (36, 48, and 60 h) have been carried out. For the convenience of description, the SnSe₂ samples prepared at different reaction times were named SnSe₂-X, where X represents the reaction time in hours.

2.2 Materials characterization

The morphologies of the prepared samples were recorded using scanning electron microscopy (SEM, Sirion 200) and transmission electron microscopy (TEM, JEOL-1400) together with high-resolution TEM (HRTEM, JEM-2100HR). The crystal structure information of the samples was analyzed by powder X-ray diffraction (XRD, Bruker D8 Advance) with Cu K α radiation and Raman spectroscopy (InVia Reflex, Renishaw) with a 532 nm wavelength incident laser. The chemical states were determined by X-ray photoelectron spectroscopy (XPS, ESCLAB 250Xi, Thermo Fisher) using Mg as the excitation source. The specific surface areas of the products were measured using a Quantachrome Autosorb automated gas sorption system and analyzed using the Brunauer–Emmett–Teller (BET) method. The electron paramagnetic resonance (EPR) spectra were measured on a JEOL JES-FA200 electron spin resonance spectrometer at 123 K.

2.3 Gas-sensing measurements

The gas sensors were fabricated by the drop-casting method as shown in Fig. S1.† In a typical process, the as-prepared SnSe₂ powder (10 mg) was dissolved in anhydrous ethanol (1 mL), followed by ultrasonic treatment for about 10 min. Then, 20 μL of the suspension was dropped onto commercial alumina substrates (7 × 14 mm) with Ag–Pd interdigital electrodes (with 5 pairs and a spacing between each pair of 200 μm) and then dried in an oven at 60 °C for 1 h.

The gas sensing characteristics were analyzed using a self-made detection system reported in our previous work.^{44,45} The real-time electrical conductance change was monitored and recorded through an electrochemical workstation (CHI 630E). The target gas was injected into the testing chamber (4 L) through a syringe, and the gas concentration in the chamber can be calculated based on the injected volume. The relative humidity (RH) was controlled using a commercial damp-heat chamber (CK-80G, Kingjo) during the sensing period. The sensing response (*S*) was defined as $S(\%) = \frac{R_g - R_a}{R_a} \times 100$, where *R_a* and *R_g* stand for the resistance of the sensor in air and the tested gas, respectively. The time taken to reach 90% resistance change after target gas on and off was defined as the response time and recovery time, respectively. The measurements were carried out in ambient air (25 °C, 40–50% RH).

3 Results and discussion

3.1 Morphology and structure

Hierarchical SnSe₂ was obtained through a one-step solvothermal process using SnCl₄·5H₂O as the tin source, SeO₂ as the selenium source, oleylamine as the solvent, and 1-DDT as a surfactant at a reaction temperature of 180 °C (as shown in Fig. 1a). To investigate the formation process of the SnSe₂ hierarchical structures, time-dependent experiments (36, 48, and 60 h) were carried out. The morphology change of SnSe₂ with various reaction times was observed by SEM analysis and could be explained by a well-studied mechanism of nanoparticle aggregation.^{43,46} During the early stage of the solvothermal process, individual nanoparticle seeds are formed and begin to coalesce to form the initial nanosheet structure (Fig. 1b and S2†). Afterwards, as “petals” of nanosheets protrude from the nanosheet assemblies, a flowerlike morphology starts to emerge (Fig. 1c). With increasing reaction time, the newly-formed SnSe₂ nanosheets could grow out vertically and then grow up, which leads to the anisotropic growth of the nanosheets into flower-like hierarchical structures (Fig. 1d and S3†). The special morphology of the individual SnSe₂ hierarchical structures was further confirmed by TEM. As shown in Fig. 1e, the TEM observations are completely consistent with the SEM observations in terms of shape and size, and it is obvious that the flower-like structure

is assembled by individual thin nanosheets as “petals” (Fig. 1f). The HRTEM image (Fig. 1g) shows a clear lattice fringe interval of 0.330 nm, corresponding to the (100) plane of hexagonal SnSe₂. It is generally accepted that flower-like hierarchical structures could provide large void spaces and active surface areas, which benefit gas adsorption and diffusion in gas sensing processes.

To investigate the crystal phases and crystallinity, the as-prepared SnSe₂ samples were characterized by XRD. As illustrated in Fig. 2a, the diffraction peaks of all the products at $2\theta = 14.41^\circ, 26.99^\circ, 30.73^\circ, 40.07^\circ, 44.21^\circ, 47.69^\circ, 50.08^\circ, 52.56^\circ$ and 57.81° match well with the peaks of the (001), (100), (011), (012), (003), (110), (111), (103) and (201) planes of hexagonal SnSe₂ (JCPDS No. 89-3197) with the space group $P\bar{3}m1$.⁴⁷ The sharp peaks without any impurity phase in XRD indicate the high crystallinity and purity of the samples. It is worth noting that the relative intensity of the diffraction peaks varies with the reaction time, implying the difference in the orientation of SnSe₂. For the SnSe₂-36 h sample, the high intensity of the (001) peak indicates that the basal planes are preferentially exposed, which is consistent with the sheet-like morphology.⁴⁸ The SnSe₂-60 h sample does not display a preferred orientation, demonstrating that the SnSe₂ nanosheet “petals” grow in different directions during the reaction process, thereby forming hierarchical structures with large void spaces. The changing trend of diffraction peak

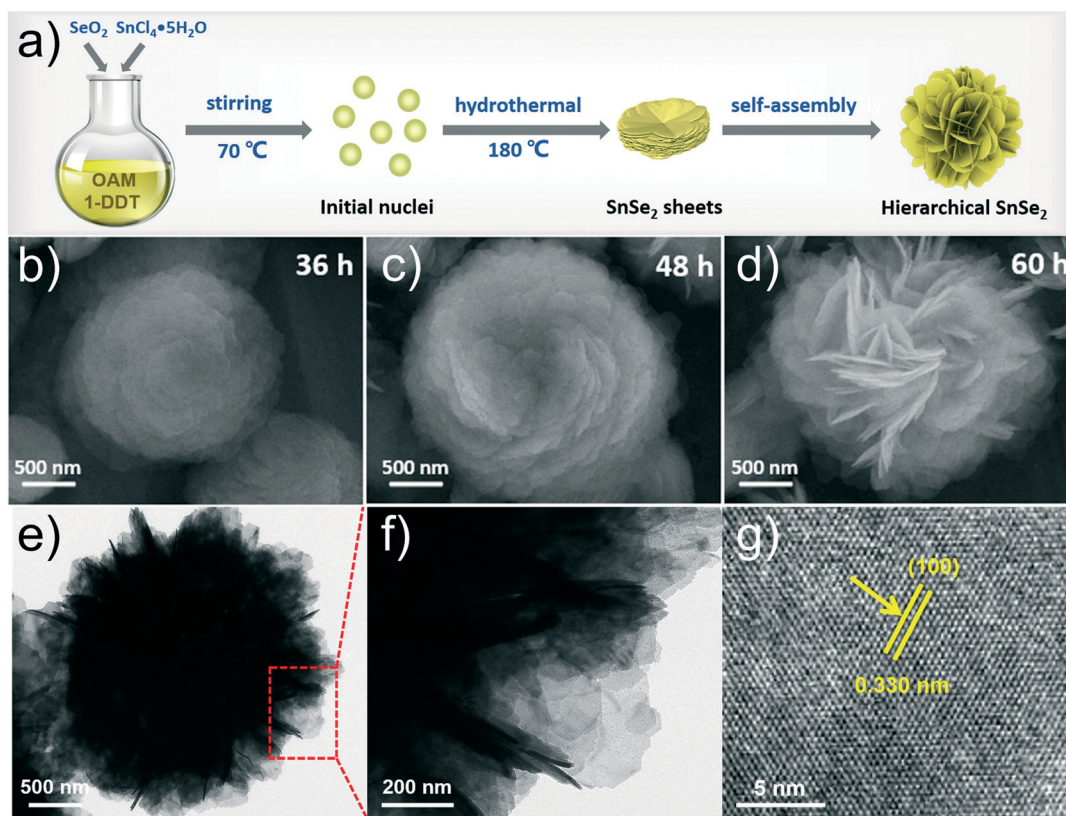


Fig. 1 (a) Schematic illustration for the synthesis process of SnSe₂ hierarchical nanostructures. SEM images of SnSe₂ with different reaction times: (b) 36 h, (c) 48 h, and (d) 60 h. (e and f) TEM and (g) HRTEM images of the SnSe₂-60 h sample.

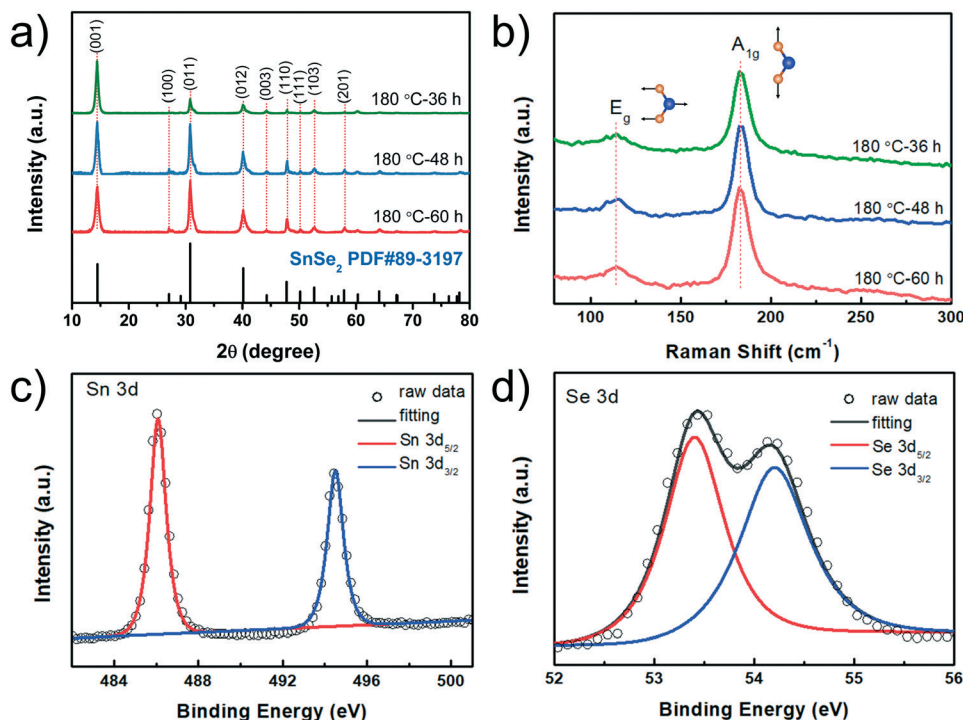


Fig. 2 (a) XRD patterns and (b) Raman spectra of the synthesized SnSe₂ with different reaction times. XPS spectra of the (c) Sn 3d orbitals and the (d) Se 3d orbitals of the SnSe₂-60 h sample.

intensity with reaction time corresponds to the above morphology characterization.

Raman spectroscopy was used to further characterize the quality of the SnSe₂ samples. Two main peaks are observed at 114 cm⁻¹ and 183 cm⁻¹ for all the SnSe₂ samples, as shown in Fig. 2b. The former peak is assigned to the E_g mode which is caused by the in-plane vibrations of the two Se atoms in opposite directions of the Sn atom. The latter peak is assigned to the A_{1g} mode which results from the vibrations of the Se atomic sheets in opposite directions of the Sn layer.^{20,49} Additionally, the surface chemical states of the hierarchical SnSe₂ structures were analyzed by XPS measurements. From the full-scale survey spectrum in Fig. S4,† the SnSe₂ only shows emissions of the Sn and Se elements with weak C and O lines, indicating the purity of the product, which is consistent with the observation from XRD and Raman analysis. The high-resolution XPS spectra of the Sn 3d and Se 3d regions are shown in Fig. 2c and d. The Sn 3d spectrum is split into two main features with the signals at 486.1 and 495.4 eV, which arise from the Sn 3d_{5/2} and Sn 3d_{3/2} orbitals of Sn⁴⁺. Similarly, the spectrum of Se 3d exhibits two strong peaks of Se 3d_{5/2} at 53.4 eV and Se 3d_{3/2} at 54.2 eV.^{50,51} All the above characterization results suggest that we have successfully fabricated high-purity SnSe₂ hierarchical structures as well as SnSe₂ nanosheets.

3.2 Gas sensing properties

The sensing properties of the SnSe₂ sensors were evaluated at room temperature by measuring the changes in resistance

upon exposure to low-concentration NO₂. The effect of the morphologies and structures on sensing performance is investigated first. Fig. 3a displays the dynamic gas sensing curves of the three sensors (labelled as SnSe₂-36, 48, and 60 h) for NO₂ concentrations ranging from 1 to 20 ppm, and Fig. 3b plots the correlation curve of the responses with NO₂ gas concentration. Rapid responses, excellent recovery characteristics, and a good linear relationship between the sensing response and NO₂ concentration can be observed for all the sensors. The optimal sensor SnSe₂-60 h exhibits a higher response value and shorter response/recovery time than SnSe₂-36 h (Fig. S5†). It is obvious that the superior sensing performance of the SnSe₂-60 h sensor could be ascribed to the special hierarchical structures and the corresponding mechanism will be discussed later. To determine the limit of detection (LOD), the SnSe₂-60 h sample was further exposed to low concentrations (from 500 to 10 ppb) of NO₂ (Fig. 4a). As shown, the sensor demonstrates a reversible response–recovery curve and high sensing response to ppb-levels of NO₂, and the lowest detected concentration reaches 10 ppb with a 20% response, which is below the acceptable ambient level of 53 ppb set by the U.S. EPA.

The selectivity of the SnSe₂ was investigated upon exposure to various test gases, including H₂S, NH₃, CH₄, CO and several volatile organic compounds (VOCs) (Fig. 4b and S6†). Clearly, the response to NO₂ is much higher than those to other gases, because NO₂ molecules adsorbed on SnSe₂ have a higher adsorption energy and charge transfer degree based on density functional theory calculations according to

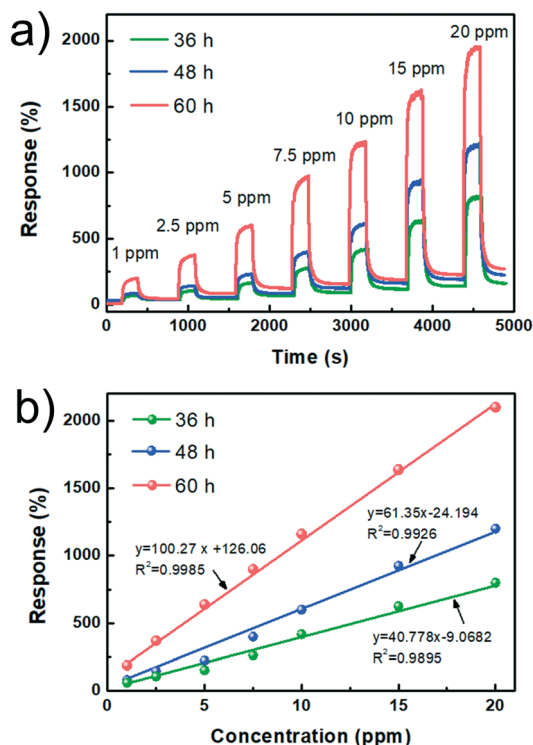


Fig. 3 Room-temperature NO₂ gas-sensing properties of sensors based on SnSe₂ with different reaction times: (a) dynamic response-recovery curves and (b) the responses of the sensors as a function of gas concentration.

a recent reported study.¹⁹ The excellent selectivity enables our gas sensors to avoid the effects of cross-sensing under practical application conditions. Besides, uniformity and repeatability are key for sensing devices in practical

applications. Thus, the sensing performances of 5 different devices based on SnSe₂ hierarchical structures were measured. As shown in Fig. S7,† the baseline of resistance varies slightly from device to device, but the sensing responses toward 10 ppm NO₂ are almost the same. Reproducibility and stability are also critical characteristics for gas sensors. Fig. 4c shows the four consecutive sensing cycles of SnSe₂-60 h for 10 ppm NO₂, where the response and recovery curves are almost identical in each trial. Moreover, this clearly shows that both the sensing response and response/recovery time are very stable as the aging time increased to 5 months. (Fig. 4d and S8†). A comparison of room-temperature NO₂ sensors based on LMDs with various nanostructures is shown in Table 1. Apparently, compared with other reported materials like MoS₂, MoSe₂, WS₂, WSe₂ and NbS₂, the hierarchical SnSe₂ in this work shows better NO₂ sensing performance including high response, rapid response kinetics along with full recovery, and low detection limit. Taking the convenient synthesis route and competitive NO₂ sensing properties into account, the SnSe₂ hierarchical structure materials have undoubtedly proved to be a distinctive candidate for constructing high-performance NO₂ sensors suitable for various fields.

Relative humidity (RH) is also an indispensable condition for the practical application of sensing devices. The effect of humidity (from 15% to 85%) on the SnSe₂ based sensors with 10 ppm NO₂ at room temperature is presented in Fig. 4e and f. It can be observed that the baseline resistance of the sensor decreases as the RH increases, which could be explained by the electron mechanism.^{59,62,63} As is known, SnSe₂ shows *n*-type semiconductor properties and the water molecules that adsorbed on the surface of the sensing materials act as electron donors. Thereby, the increase in humidity leads to an increase in the density of main carriers (electrons) and a decrease in

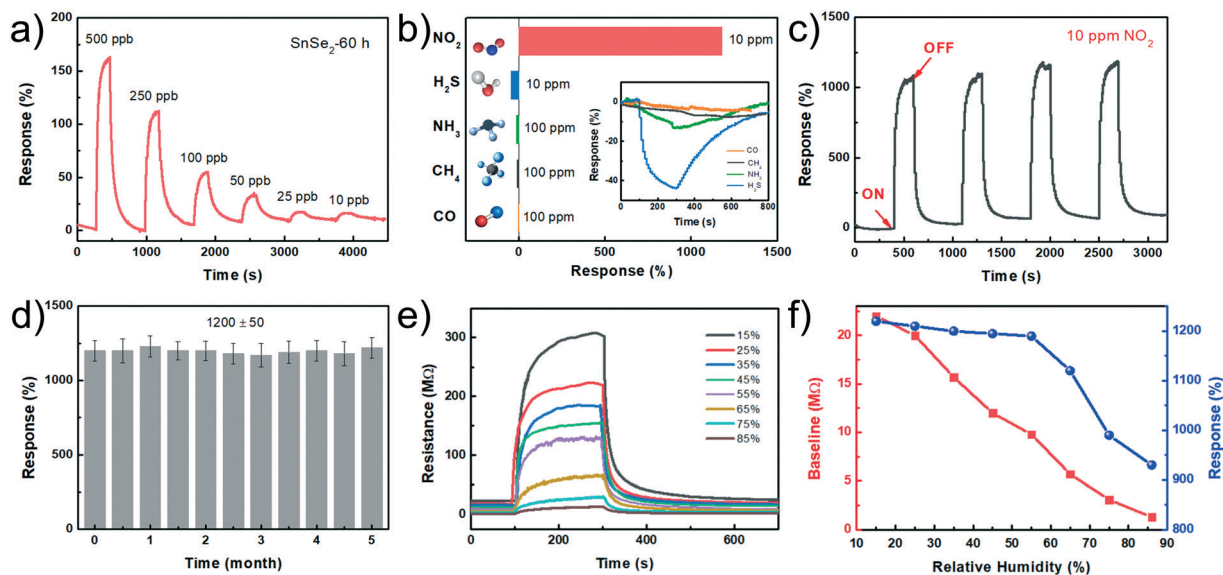


Fig. 4 Sensing performance of SnSe₂ hierarchical structures: (a) dynamic response-recovery curves for ppb-level NO₂. (b) Selectivity response toward H₂S, NH₃, CH₄, and CO. (c) Four successive sensing cycles for 10 ppm NO₂. (d) Long-term stability with 10 ppm NO₂ within five months. (e) The resistance variations and (f) baseline resistance and sensing response to 10 ppm NO₂ under different relative humidity conditions (15–85%).

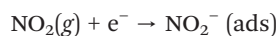
Table 1 Comparison of sensing performance of the SnSe₂ hierarchical structures with those of previously reported NO₂ gas sensors based on LMDs at room temperature

Material	Morphology	Concentration (ppm)	Response (%)	Response/recovery time (s/s)	Detection limit (ppb)	Ref.
SnSe ₂	Hierarchical structures	10	1200	50/55	10	This work
SnSe ₂	Flakes	8	38.2	~150/200	136	21
SnSe ₂	Flakes	1	60	142/935	100	19
SnS ₂	Nanograins	5	300	1000/2000	409	52
MoS ₂	Bilayer film	1	2.6	700/300	1000	53
MoS ₂	Flakes	100	24	249/unrecoverable	—	54
MoS ₂	Flakes	500	350	180/480	—	55
MoSe ₂	Single layer	5	40	450/600	—	56
MoSe ₂	Nanosheets	10	1500	~90/>1200	50	57
WS ₂	Nanosheets	5	68	200/>600	100	58
WSe ₂	Nanosheets	10	1000	50/1000	50	59
WSe ₂	Flakes	500	4140	900/>5000	—	60
NbS ₂	Nanosheets	5	18	~3000/~9000	241	61

resistance. Additionally, with the relative humidity increasing, the sensing response value becomes lower. One possible reason is that the absorbed water molecules would occupy some adsorption sites on the surface of SnSe₂, thus leading to less active sites to attract NO₂. Besides, NO₂ molecules are more easily consumed by water vapor, which is particularly apparent under high humidity conditions. It is worth mentioning that under the moderate humidity conditions (15% to 55%), although the absorbed water molecules would decrease the resistance of the sensing materials, they could not occupy a large number of active sites. The target NO₂ gas molecules could still spontaneously adsorb on the surface of the materials and react with SnSe₂. Therefore, the relative response attenuation of the gas sensors is slight and negligible (from 1230% to 1180%), indicating the outstanding stability of the SnSe₂ gas sensors.

3.3 Gas sensing mechanism

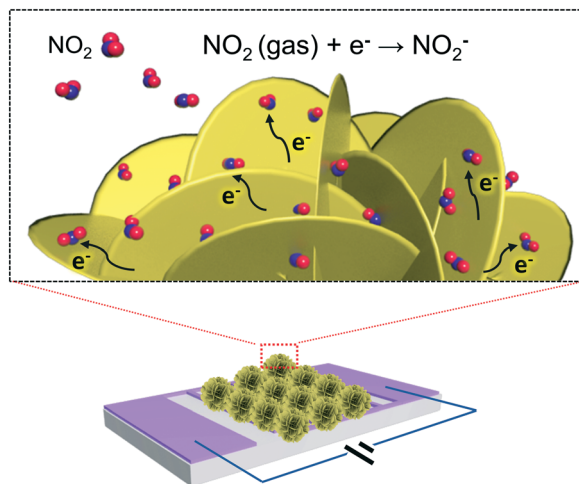
The basic sensing principle of 2D LMD materials relies upon the charge transfer process between the sensing materials and gas molecules.^{12,14,19} As shown in Fig. S9,† when *n*-type SnSe₂ is exposed to oxidizing NO₂ gas, the electrophilic NO₂ molecules that are spontaneously adsorbed on the surface of SnSe₂ will extract electrons from the conduction band of SnSe₂ to form adsorbed NO₂⁻. As a result, the electron concentration decreases and subsequently the resistance of the sensor increases. The process could be expressed by the following equation:



The enhanced sensing performance of hierarchical SnSe₂ could be attributed to the following factors. Firstly, the enlarged specific area caused by the hierarchical structure endows the SnSe₂ sensors with more surface reactive sites for NO₂ adsorption, thus leading to the improved response value. The BET surface areas of the three different SnSe₂ samples were analyzed by N₂ adsorption-desorption analyses (Fig. S10†). The flower-like hierarchical structure gives rise to the highest specific surface area of 8.48 m² g⁻¹ compared with

the nanosheets with 3.76 m² g⁻¹ and 5.07 m² g⁻¹, in accordance with the response tendency (Fig. 3). Secondly, defects are easy to introduce during the solvothermal method. Electron paramagnetic resonance (EPR) spectra were measured to verify the presence of Se vacancies in the SnSe₂ samples. As shown in Fig. S11,† the EPR signal at *g* = 2.003 was caused by the trapped electrons from the Se vacancies,^{64,65} whereas the SnSe₂-60 h sample shows a much stronger signal at the same position, obviously indicating that the hierarchical SnSe₂ possesses a relatively higher concentration of Se vacancies compared to the SnSe₂ nanosheets. These defects are often regarded as active sites that facilitate gas adsorption, thus achieving a higher sensing response.^{66,67} Furthermore, some previous studies have reported that SnSe₂ would spontaneously form a subnanometric SnO₂ skin once exposed to air due to oxidation driven by Se vacancies.^{22,68} To investigate the oxidation degree of the hierarchical SnSe₂ sample after aging for 5 months, the sample was characterized by XRD and XPS measurements. As shown in Fig. S12,† no diffraction peaks of SnO₂ are observed in the XRD results. However, two additional peaks belonging to SnO₂ could be seen in the high-resolution Sn core level (3d_{5/2}) and O 1s spectra, which indicates that SnSe₂ is slightly oxidized after 5 months. Nevertheless, the sensing properties including the response value and response/recovery time toward 10 ppm NO₂ of the hierarchical SnSe₂ sensor are very stable as the aging time increased to 5 months (as shown in Fig. S8†), demonstrating that the slight oxidation has no significant effect on the sensing performance.

In addition, the better response and recovery times of hierarchical SnSe₂ could be ascribed to two aspects. First, compared to the stacked nanosheets, the hierarchical structures have higher efficiency. As schematically illustrated in Scheme 1, the well-defined interior voids between adjacent nanosheets could serve as unimpeded flow passages. When the hierarchical SnSe₂ is exposed to target gases, the gas molecules easily spread inward through the well-aligned throughpores smoothly. Upon re-exposure to air, the desorption of gas molecules will occur in a shorter period of time. Therefore, although more gas



Scheme 1 Schematic illustration of the sensing mechanism of SnSe₂ hierarchical structures exposed to NO₂.

molecules are adsorbed on the surface of hierarchical SnSe₂, the gas diffusion is more effective. In other words, the utilization factor of the sensing film is higher for the hierarchical structures.^{34,35} Besides, the intrinsic electrical properties and band structure of materials have an effect on the sensing performance. SnSe₂ has a narrow bandgap (~1.3 eV) and high intrinsic electron mobility (462.6 cm² V⁻¹ s⁻¹ at 300 K).⁶⁹ These properties provide SnSe₂ with good electrical conductivity and boosted charge transfer ability, which might accelerate the response/recovery process to a certain extent. Consequently, the unique hierarchical structure and inherent electronic properties of SnSe₂ are advantageous to acquire a high sensing response as well as a high response/recovery speed.

4 Conclusions

In summary, flower-like SnSe₂ hierarchical structures were successfully synthesized *via* a solvothermal method and exhibited improved room-temperature NO₂ gas sensing performance. Attributed to the numerous interconnected nanosheets, the hierarchical structures demonstrate a large accessible active area and well-defined interior voids, which promote gas adsorption and transportation. Consequently, gas sensors based on hierarchical SnSe₂ demonstrate an ultralow detection limit (10 ppb), high response (1200% at 10 ppm), and remarkable long-term stability (5 months). The construction of hierarchical structures offers new opportunities for surface morphology control to enhance the gas sensing performance of SnSe₂.

Conflicts of interest

There are no conflicts to declare.

Acknowledgements

This work was supported by the National Key Research and Development Program of China (2019YFA0705201), the

National Natural Science Foundation of China (No. 52072093 and 51802058), the Applied Technology Research and Development Program of Heilongjiang Province (No. GY2018ZB0046), and the China Postdoctoral Science Foundation funded project.

Notes and references

- 1 R. Atkinson, *Atmos. Environ.*, 2000, **34**, 2063–2101.
- 2 M. Guarnieri and J. R. Balmes, *Lancet*, 2014, **383**, 1581–1592.
- 3 J. Z. Ou, C. K. Yao, A. Rotbart, J. G. Muir, P. R. Gibson and K. Kalantar-zadeh, *Trends Biotechnol.*, 2015, **33**, 208–213.
- 4 A.-M. Andringa, J. R. Meijboom, E. C. P. Smits, S. G. J. Mathijssen, P. W. M. Blom and D. M. de Leeuw, *Adv. Funct. Mater.*, 2011, **21**, 100–107.
- 5 J. Hu, C. Zou, Y. Su, M. Li, N. Hu, H. Ni, Z. Yang and Y. Zhang, *J. Mater. Chem. C*, 2017, **5**, 6862–6871.
- 6 R. A. Potyrailo, *Chem. Rev.*, 2016, **116**, 11877–11923.
- 7 M. Swan, *J. Sens. Actuator Netw.*, 2012, **1**, 217–253.
- 8 A. Baranov, D. Spirjakina, S. Akbari and A. Somov, *Sens. Actuators, A*, 2015, **233**, 279–289.
- 9 J.-H. Lee, *Sens. Actuators, B*, 2009, **140**, 319–336.
- 10 Z. Li, H. Li, Z. Wu, M. Wang, J. Luo, H. Torun, P. Hu, C. Yang, M. Grundmann, X. Liu and Y. Fu, *Mater. Horiz.*, 2019, **6**, 470–506.
- 11 C. Baratto, R. Kumar, E. Comini, M. Ferroni and M. Campanini, *Nanotechnology*, 2017, **28**, 465502.
- 12 E. Lee, Y. S. Yoon and D. J. Kim, *ACS Sens.*, 2018, **3**, 2045–2060.
- 13 B. L. Li, J. Wang, H. L. Zou, S. Garaj, C. T. Lim, J. Xie, N. B. Li and D. T. Leong, *Adv. Funct. Mater.*, 2016, **26**, 7034–7056.
- 14 X. Liu, T. Ma, N. Pinna and J. Zhang, *Adv. Funct. Mater.*, 2017, **27**, 1702168.
- 15 J. Ping, Z. Fan, M. Sindoro, Y. Ying and H. Zhang, *Adv. Funct. Mater.*, 2017, **27**, 1605817.
- 16 L. Zhang, K. Khan, J. Zou, H. Zhang and Y. Li, *Adv. Mater. Interfaces*, 2019, **6**, 1901329.
- 17 M. Chen, Z. Wang, X. Ge, Z. Wang, K. Fujisawa, J. Xia, Q. Zeng, K. Li, T. Zhang, Q. Zhang, M. Chen, N. Zhang, T. Wu, S. Ma, G. Gu, Z. Shen, L. Liu, Z. Liu, M. Terrones and L. Wei, *Matter*, 2020, **2**, 666–679.
- 18 M. Chen, J. Xia, J. Zhou, Q. Zeng, K. Li, K. Fujisawa, W. Fu, T. Zhang, J. Zhang, Z. Wang, Z. Wang, X. Jia, M. Terrones, Z. X. Shen, Z. Liu and L. Wei, *ACS Nano*, 2017, **11**, 9191–9199.
- 19 O. L. Camargo Moreira, W. Y. Cheng, H. R. Fuh, W. C. Chien, W. Yan, H. Fei, H. Xu, D. Zhang, Y. Chen, Y. Zhao, Y. Lv, G. Wu, C. Lv, S. K. Arora, O. C. C. C. Heng, C. R. Chang and H. C. Wu, *ACS Sens.*, 2019, **4**, 2546–2552.
- 20 M. Chen, Z. Li, W. Li, C. Shan, W. Li, K. Li, G. Gu, Y. Feng, G. Zhong, L. Wei and C. Yang, *Nanotechnology*, 2018, **29**, 455501.
- 21 X. Li, W. Liu, B. Huang, H. Liu and X. Li, *J. Mater. Chem. C*, 2020, **8**, 15804–15815.
- 22 V. Paolucci, G. D'Olimpio, C. N. Kuo, C. S. Lue, D. W. Boukhvalov, C. Cantalini and A. Politano, *ACS Appl. Mater. Interfaces*, 2020, **12**, 34362–34369.

- 23 M. Pawar, S. Kadam and D. J. Late, *ChemistrySelect*, 2017, **2**, 4068–4075.
- 24 X. Wang, Y. Liu, J. Dai, Q. Chen, X. Huang and W. Huang, *Chemistry*, 2020, **26**, 3870–3876.
- 25 J. Chen, D. M. Hamann, D. Choi, N. Poudel, L. Shen, L. Shi, D. C. Johnson and S. Cronin, *Nano Lett.*, 2018, **18**, 6876–6881.
- 26 L. Lee, C.-W. Chen, A. Manikandan, S.-H. Lee, Z. M. Wang and Y.-L. Chueh, *Nano Energy*, 2018, **44**, 419–429.
- 27 S. Veeralingam, P. Sahatiya and S. Badhulika, *Sens. Actuators, B*, 2019, **297**, 126725.
- 28 Z. Wei, L. Wang, M. Zhuo, W. Ni, H. Wang and J. Ma, *J. Mater. Chem. A*, 2018, **6**, 12185–12214.
- 29 H. Chen, R. Liu, Y. Wu, J. Cao, J. Chen, Y. Hou, Y. Guo, R. Khatoun, L. Chen, Q. Zhang, Q. He and J. Lu, *Chem. Eng. J.*, 2021, **407**, 126073.
- 30 B. Pejjai, V. R. Minnam Reddy, S. Gedi and C. Park, *Int. J. Hydrogen Energy*, 2017, **42**, 2790–2831.
- 31 M. H. Sun, S. Z. Huang, L. H. Chen, Y. Li, X. Y. Yang, Z. Y. Yuan and B. L. Su, *Chem. Soc. Rev.*, 2016, **45**, 3479–3563.
- 32 H. Tang, L. N. Sacco, S. Vollebregt, H. Ye, X. Fan and G. Zhang, *J. Mater. Chem. A*, 2020, **8**, 24943–24976.
- 33 W. Ge, S. Jiao, Z. Chang, X. He and Y. Li, *ACS Appl. Mater. Interfaces*, 2020, **12**, 13200–13207.
- 34 Z. Song, H. Chen, S. Bao, Z. Xie, Q. Kuang and L. Zheng, *J. Mater. Chem. A*, 2020, **8**, 3754–3762.
- 35 W. Tan, J. Tan, L. Li, M. Dun and X. Huang, *Sens. Actuators, B*, 2017, **249**, 66–75.
- 36 S. Wang, J. Yang, H. Zhang, Y. Wang, X. Gao, L. Wang and Z. Zhu, *Sens. Actuators, B*, 2015, **207**, 83–89.
- 37 S. Wei, Y. Xing, Y. Li, Y. Zhao, W. Du and M. Zhou, *Vacuum*, 2016, **129**, 13–19.
- 38 D. Liu, Z. Tang and Z. Zhang, *Sens. Actuators, B*, 2018, **273**, 473–479.
- 39 Y. Zhang, W. Zeng and Y. Li, *Appl. Surf. Sci.*, 2018, **455**, 276–282.
- 40 Y. Zhang, W. Zeng and Y. Li, *J. Alloys Compd.*, 2018, **749**, 355–362.
- 41 W. Li, K. He, D. Zhang, N. Li, Y. Hou, G. Cheng, W. Li, F. Sui, Y. Dai, H. Luo, Y. Feng, L. Wei, W. Li, G. Zhong, M. Chen and C. Yang, *ACS Appl. Energy Mater.*, 2019, **2**, 2803–2809.
- 42 W. Li, L. Xiong, N. Li, S. Pang, G. Xu, C. Yi, Z. Wang, G. Gu, K. Li, W. Li, L. Wei, G. Li, C. Yang and M. Chen, *J. Mater. Chem. C*, 2019, **7**, 10179–10186.
- 43 P. Ramasamy, P. Manivasakan and J. Kim, *CrystEngComm*, 2015, **17**, 807–813.
- 44 Q. Sun, J. Hao, S. Zheng, P. Wan, J. Li, D. Zhang, Y. Li, T. Wang and Y. Wang, *Nanotechnology*, 2020, **31**, 425502.
- 45 S. Zheng, J. Sun, J. Hao, Q. Sun, P. Wan, Y. Li, X. Zhou, Y. Yuan, X. Zhang and Y. Wang, *Nanotechnology*, 2021, **32**, 155505.
- 46 D. Dimitri, S.-I. In and R. E. Schaak, *ACS Nano*, 2011, **5**, 8852–8860.
- 47 Y. Zhang, Y. Liu, K. H. Lim, C. Xing, M. Li, T. Zhang, P. Tang, J. Arbiol, J. Llorca, K. M. Ng, M. Ibanez, P. Guardia, M. Prato, D. Cadavid and A. Cabot, *Angew. Chem., Int. Ed.*, 2018, **57**, 17063–17068.
- 48 R. K. Rai, S. Islam, A. Roy, G. Agrawal, A. K. Singh, A. Ghosh and N. Ravishankar, *Nanoscale*, 2019, **11**, 870–877.
- 49 D. Yin, Y. Liu, C. Dun, D. L. Carroll and M. T. Swihart, *Nanoscale*, 2018, **10**, 2533–2541.
- 50 E. P. Mukhokosi, S. B. Krupanidhi and K. K. Nanda, *Sci. Rep.*, 2017, **7**, 15215.
- 51 T. Xu, Y. Han, L. Lin, J. Xu, Q. Fu, H. He, B. Song, Q. Gai and X. Wang, *J. Alloys Compd.*, 2019, **790**, 941–946.
- 52 K. C. Kwon, J. M. Suh, T. H. Lee, K. S. Choi, K. Hong, Y. G. Song, Y. S. Shim, M. Shokouhimehr, C. Y. Kang, S. Y. Kim and H. W. Jang, *ACS Sens.*, 2019, **4**, 678–686.
- 53 T. Xu, Y. Pei, Y. Liu, D. Wu, Z. Shi, J. Xu, Y. Tian and X. Li, *J. Alloys Compd.*, 2017, **725**, 253–259.
- 54 R. Kumar, N. Goel and M. Kumar, *ACS Sens.*, 2017, **2**, 1744–1752.
- 55 Y. Zhao, J. G. Song, G. H. Ryu, K. Y. Ko, W. J. Woo, Y. Kim, D. Kim, J. H. Lim, S. Lee, Z. Lee, J. Park and H. Kim, *Nanoscale*, 2018, **10**, 9338–9345.
- 56 S. Zhang, T. H. Nguyen, W. Zhang, Y. Park and W. Yang, *Appl. Phys. Lett.*, 2017, **111**, 161603.
- 57 X. Chen, X. Chen, Y. Han, C. Su, M. Zeng, N. Hu, Y. Su, Z. Zhou, H. Wei and Z. Yang, *Nanotechnology*, 2019, **30**, 445503.
- 58 T. Xu, Y. Liu, Y. Pei, Y. Chen, Z. Jiang, Z. Shi, J. Xu, D. Wu, Y. Tian and X. Li, *Sens. Actuators, B*, 2018, **259**, 789–796.
- 59 R. Guo, Y. Han, C. Su, X. Chen, M. Zeng, N. Hu, Y. Su, Z. Zhou, H. Wei and Z. Yang, *Sens. Actuators, B*, 2019, **300**, 127013.
- 60 K. Y. Ko, K. Park, S. Lee, Y. Kim, W. J. Woo, D. Kim, J. G. Song, J. Park and H. Kim, *ACS Appl. Mater. Interfaces*, 2018, **10**, 23910–23917.
- 61 Y. Kim, K. C. Kwon, S. Kang, C. Kim, T. H. Kim, S. P. Hong, S. Y. Park, J. M. Suh, M. J. Choi, S. Han and H. W. Jang, *ACS Sens.*, 2019, **4**, 2395–2402.
- 62 Y. Han, Y. Liu, C. Su, S. Wang, H. Li, M. Zeng, N. Hu, Y. Su, Z. Zhou, H. Wei and Z. Yang, *Sens. Actuators, B*, 2019, **296**, 126666.
- 63 Y. Li, Z. Song, Y. Li, S. Chen, S. Li, Y. Li, H. Wang and Z. Wang, *Sens. Actuators, B*, 2019, **282**, 259–267.
- 64 Y. Sun, J. Meng, H. Ju, J. Zhu, Q. Li and Q. Yang, *J. Mater. Chem. A*, 2018, **6**, 22526–22533.
- 65 L. Zhang, C. Lu, F. Ye, R. Pang, Y. Liu, Z. Wu, Z. Shao, Z. Sun and L. Hu, *Adv. Mater.*, 2021, **33**, 2007523.
- 66 W. Y. Cheng, H. R. Fuh and C. R. Chang, *Appl. Sci.*, 2020, **10**, 1623.
- 67 Z. Hu, Z. Wu, C. Han, J. He, Z. Ni and W. Chen, *Chem. Soc. Rev.*, 2018, **47**, 3100–3128.
- 68 G. D'Olimpio, F. Genuzio, T. O. Mentis, V. Paolucci, C. N. Kuo, A. Al Taleb, C. S. Lue, P. Torelli, D. Farias, A. Locatelli, D. W. Boukhvalov, C. Cantalini and A. Politano, *J. Phys. Chem. Lett.*, 2020, **11**, 9003–9011.
- 69 W. Zhang, Z. Huang, W. Zhang and Y. Li, *Nano Res.*, 2014, **7**, 1731–1737.